Journal of Environmental Management 371 (2024) 123178

Contents lists available at ScienceDirect

Journal of Environmental Management

journal homepage: www.elsevier.com/locate/jenvman

Research article

Advancing solar wastewater treatment: A photocatalytic process via green ZnO/g-C_3N_4 coatings and concentrated sunlight – Comprehensive insights into ciprofloxacin antibiotic inactivation

Asma El Golli [a], Davide Losa [b], Claudio Gioia [a], Murilo Fendrich [a], Om Prakash Bajpai [a], Olivier Jousson [b], Michele Orlandi [a,*], Antonio Miotello [a]

[a] Physics Department, University of Trento, via Sommarive 14, 38123, Povo, Trento, Italy
[b] Department of Cellular, Computational and Integrative Biology, CIBIO, University of Trento, via Sommarive 9, 38123, Povo, Trento, Italy

A B S T R A C T

In this study, a sustainable method employing concentrated sunlight to achieve environmental remediation of wastewater, contaminated by Ciprofloxacin antibiotic (CIP), is thoroughly investigated. A green ZnO/g-C_3N_4 nanocomposite (NC) is used as a photocatalyst coating on glass to investigate the inactivation of CIP in water, in a flow-reactor configuration at small-prototype scale (10 liters/h, catalyst area 187.5 cm^2). ZnO/g-C_3N_4 NC coatings were obtained by an *in-situ* thermal condensation process coupled with a green synthesis protocol and deposited on glass, via a simple drop casting method. Morphological and structural analyses of synthesized composites were performed with Fourier-Transform Infrared (FTIR) Spectroscopy, Scanning Electron Microscopy (SEM), Energy-Dispersive X-ray (EDX) and X-ray diffraction (XRD) techniques, while optical properties were studied with Diffuse Reflectance Spectroscopy (DRS). The degradation of CIP was first tested at a lab scale under simulated sunlight and then studied under sunlight in a parabolic trough concentrator (PTC). Suitable degradation of CIP (100%) was observed at 210 min via High-Performance Liquid Chromatography (HPLC) and the by-products were determined by Liquid Chromatography-Mass Spectroscopy (LC–MS). Microbiological tests revealed the absence of antibacterial activity in CIP water treated with ZnO/g-C_3N_4 NC photocatalyst against *Staphylococcus aureus*, *Pseudomonas aeruginosa,* and *Priestia megaterium*. Our results directly demonstrate the effective inactivation of CIP with a process designed for sustainability both in terms of energy input (solar) and scalability of materials. Also, the small-prototype scale of this investigation provides insights into the challenges arising from the perspective scale-up to an industrial application, aimed at antibiotics inactivation in wastewater and thus helping to prevent the spread of antimicrobial resistance (AMR).

1. Introduction

The release of effluents, often containing various toxic compounds, into aquatic systems leads to significant water pollution (Ngullie et al., 2020; Chidhambaram and Ravichandran, 2017; Bora and Mewada, 2017). Pharmaceutical products have been identified in urban wastewaters and surface waters worldwide, including antibiotics, which represent a crucial class of chemicals extensively employed in both human and veterinary medicine. The global usage of antibiotics annually ranges from 100,000 to 200,000 tons, with approximately 10,200 tons utilized in Europe and nearly 23,000 tons in the USA (Wise, 2002; Salma et al., 2016). Given their wide application, quinolones and their metabolites frequently reach the environment in their pharmacologically active state (Watkinson et al., 2007). Ciprofloxacin (CIP) is notably employed in veterinary and agricultural practices, but primarily for the treatment of urinary tract infections (Shariati et al., 2022). Given that humans and animals can metabolize only a minimal quantity of CIP, this antibiotic has been identified in hospital wastewaters (Hartmann et al., 1998; Van Doorslaer et al., 2014) and even in the effluents of wastewater treatment plants (WWTP), though very much diluted (Le-Minh et al., 2010). The persistence of quinolone residues in the environment has the potential to contribute to the emergence of bacterial resistance, posing a risk of harmful effects on both fauna and flora and causing significant damage to aquatic ecosystems and human health. Consequently, it is strategically crucial to minimize the release of quinolones into the environment (Salma et al., 2016; Jingyu et al., 2019). Combined with its stable chemical structure and resistance to biological degradation, along with its resistance to removal through conventional waste treatment processes, CIP inactivation has become exceptionally challenging, necessitating urgent and specific attention. Thus, it is imperative to devise innovative and straightforward methods for an efficient treatment (Jingyu et al., 2019; Uma et al., 2017; Apreja et al., 2022; Al-Buriahi et al., 2022; Husain Khan et al., 2023). These could be either aimed at treating general wastewaters or more specifically targeted at effluents coming from contamination sources, such as hospitals or pharmaceutical industries (Akhil et al., 2021). This latter case is likely to be

* Corresponding author.
E-mail address: michele.orlandi@unitn.it (M. Orlandi).

https://doi.org/10.1016/j.jenvman.2024.123178
Received 1 July 2024; Received in revised form 14 October 2024; Accepted 31 October 2024

considered more interesting for perspective applications, as concentrations are expected to be significantly higher. For example, during an investigation for a case study in northern Italy, CIP was found to be between 10 and 20 times more concentrated in hospital effluents than in WWTP influents or effluents (Verlicchi et al., 2012).

In this context, various lines of research exist for addressing contaminated water, but solar-light-induced photocatalysis stands out as an environmentally friendly, cost-efficient, and sustainable approach. Its global appeal stems from its reliance on abundant solar energy. Indeed, recent progress in solar technology, especially the adoption of low-cost solar concentrators in advancing solar-driven photocatalysis techniques, has generated noteworthy interest (El Golli et al., 2021). A recent contribution (El Golli et al., 2024) from our lab reports on the design and implementation of a PTC, evaluating both the technical efficiency and economic feasibility of the solar wastewater treatment for two case-studies, CIP and textile dyes, suggesting a way forward for solar wastewater treatments.

Typically, the photocatalytic performance is dictated by inherent physicochemical properties of the photocatalysts, such as surface area, pore size, morphological structures, extension of the band-gap and alignment of the band-edges with the oxidation and reduction processes that occur in photocatalytic reactions (Ngullie et al., 2020; Guan et al., 2019; Suhag et al., 2023). Zinc oxide (ZnO) stands out as a metal oxide semiconductor, exhibiting high chemical, thermal, and mechanical stability, nontoxic nature, and cost-effectiveness (Luu Thi et al., 2021). Nevertheless, the photocatalytic activity of ZnO is confined to the ultraviolet region due to its broad bandgap and high recombination rates (Yu et al., 2023). Recently, graphitic carbon nitride (g-C_3N_4), has garnered extensive interest for applications in hydrogen generation and the degradation of environmental pollutants (Chidhambaram and Ravichandran, 2017; Bajpai et al., 2023). This is due to its narrow band gap (2.7 eV), layered structure, remarkable stability (chemical inertness and water resistivity), π-conjugation, and well-suited band alignment (Uma et al., 2017; Luu Thi et al., 2021; MEENA et al., 2022). Indeed, the layered configuration of g-C_3N_4 provides abundant active sites for binding, allowing several organic and inorganic substances to adhere (Chidhambaram and Ravichandran, 2017). Interestingly, the combination of g-C_3N_4 with metal oxide semiconductors is reported to facilitate efficient interfacial charge transfer (Uma et al., 2017; Fendrich et al., 2023). In particular, the integration of ZnO with g-C_3N_4 leads to an effective heterostructure with visible-light reponse (Luu Thi et al., 2021; MEENA et al., 2022; Van Thuan et al., 2022).

Despite the impressive photocatalytic activity of the powdered catalyst, the recovery of the catalyst post-treatment is a complex process demanding careful attention and expensive equipment (Uma et al., 2017). The use of photocatalysts in the form of coatings is then the main way to avoid subsequent recovery. Nevertheless, there is a scarcity of reports in existing literature regarding the fabrication of a highly active ZnO/g-C_3N_4 coating (MEENA et al., 2022). While methods like hydrothermal, electron beam evaporation, and magnetron sputtering are reported for coatings deposition, here we employ the drop-casting technique to produce ZnO/g-C_3N_4 coatings because of its simplicity, cost-effectiveness, and ease of handling (Uma et al., 2017). In addition, in this work we produce ZnO/g-C_3N_4 nanocomposite (NC) photocatalysts via a green synthesis approach where garlic (*Allium Sativum*) extract is employed for both reducing and capping agents in the synthesis of ZnO nanoparticles (NPs), thus avoiding organic solvents or toxic chemicals (Lizundia et al., 2022; El Golli et al., 2023).

We then applied the coatings in a scalable process, characterized by sustainability on multiple levels (materials and energy input), to tackle the environmental issue of CIP water contamination. The inactivation of CIP was initially tested through a lab-scale simulated sunlight process and then, for scale-up perspectives, operating with an outdoor prototype (10 liters/h, catalyst area 187.5 cm^2) exploiting concentrated sunlight. Since antibiotic inactivation may often result even from partial transformation of the antibiotic structure, the effectiveness of the process was finally evaluated by microbiological tests: the residual antibacterial activity of the CIP water sampled after solar photocatalytic treatment was assessed on *Staphylococcus aureus*, *Pseudomonas aeruginosa*, *Priestia megaterium* and *Escherichia coli* cultures.

In this study a model concentration of 10 ppm CIP was used: while higher than the concentrations reported for WWTP effluents, it allowed us to elucidate reaction mechanisms and better follow kinetics. Also, the ultimate aim will be to treat real wastewaters at an early stage, where concentrations are likely higher than those reported for effluents and closer to the range investigated here. In this context, our study provides highly valuable insights that lay the groundwork for the final steps towards application. In particular, we contribute to go beyond the state of the art in two ways: (a) we provide a flow-reactor-compatible photoactive coating obtained by sustainable materials and fabrication methods; (b) building on this, we devise and demonstrate, both at the lab-scale and in a scaled-up version, a solar-powered treatment process to inactivate CIP, investigating the reaction mechanism and directly evaluating the residual antibacterial activity.

2. Materials and methods

2.1. Materials and reagents

Zinc oxide NPs were obtained with zinc nitrate ($Zn(NO_3)_2.6H_2O$, Sigma-Aldrich, ≥99% purity), *Allium Sativum* (commercial quality). Melamine ($C_3H_6N_6$, Sigma-Aldrich, purity >99%, 126.12 g/mol) was used as a g-C_3N_4 precursor. Ethanol absolute (VWR, purity 97%, 46.08 g/mol) was used as a dispersing agent for ZnO/melamine precursor for the coatings synthesis. Ciprofloxacin HCl ($C_{17}H_{18}FN_3O_3$, Standard PHR1044-1G Sigma-Aldrich, purity 99%, 385.82 g/mol) was employed as the water model pollutant in photocatalysis experiments. Lysogeny broth (LB, Sigma-Aldrich, composition: tryptone 10 g/L, yeast extract 5 g/L, NaCl 5 g/L) was the medium for bacterial cultures.

2.2. Preparation of ZnO/g-C_3N_4 NC coatings

The *in-situ* hydrothermal growth of ZnO/g-C_3N_4 NC coating started by synthesizing the ZnO NPs. The methodology follows a protocol adapted from literature (El Golli et al., 2021; Md Rosli et al., 2018). Briefly, 20g of sliced *Allium Sativum* (garlic) were boiled in 100 mL of deionized water at 80 °C and stirred at 900 rpm for 20 min to obtain a plant extract. The extract was naturally cooled to room temperature and filtered (Whatman paper n∘ 1) resulting in a total of 60 mL extract available for the NP synthesis. Afterward, 6g zinc nitrate was added to the 60 ml extract, stirred at 400 rpm for 20 min, and heated at 60 °C. The mix was dried at 110 °C for 6h in air circulated oven. Lastly, the obtained powder was washed with isopropanol and submitted to calcination at 500 °C in a muffle furnace for 4 h resulting in the ZnO NPs. The obtained ZnO NPs were then mixed in ethanol with melamine, the precursor for g-C_3N_4. The mass ratios of ZnO/Melamine were: 1:10, 1:20, and 1:60. The chosen ratios are aligned with the optimization criteria established in previous studies. The obtained g-C3N4, here reproduced and utilized, corresponds roughly to a 10% conversion yield of the melamine precursor. The selected ratios provided acceptable mechanical stability of the resulting coatings, while outside this range poor adhesion and/or delamination are generally observed (Fendrich et al., 2023; Thangavelu et al., 2023, 2024).

All three solutions were sonicated, stirred, and dropwise cast on top of precleaned glass slides (75 mm × 25 mm). After the dropwise casting of the solutions, the coatings were dried for 20 min at room temperature to remove solvent residues, followed by thermal condensation for in-situ formation of g-C_3N_4 on the ZnO structure at a temperature of 550 °C for 60 min inside a covered crucible in the muffle furnace at heating rate 9 °C/min (Bajpai et al., 2023). The coated glass slides where produced in batches of 10 for use within the flow reactor coupled to the solar concentrator. A scheme of the overall synthesis procedure is reported in

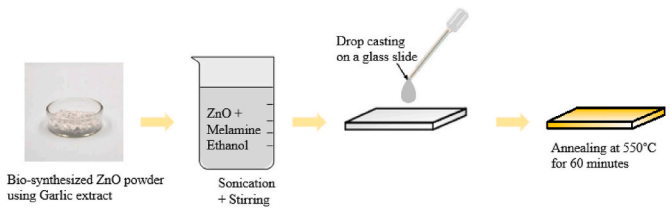

Fig. 1. – ZnO/g-C_3N_4 NC coatings synthesis.

Fig. 1.

2.3. Materials characterization

A field emission Scanning Electron Microscope (FESEM, JSM 7001 F, JEOL) equipped with Energy-Dispersive X-ray Spectroscopy analysis (EDXS, Oxford INCA PentaFET- × 3) was used to investigate coating morphology, thickness, and atomic composition. The Infrared spectroscopic analysis was performed via a JASCO 4600 instrument (Easton, PA, USA) in the range of 4000–400 cm^{-1} to confirm the presence of specific functional groups on the prepared ZnO/g-C_3N_4 coatings. UV–Vis was recorded using an integrating sphere in the total reflectance mode in the wavelengths range 200–800 nm (Varian CARY 5000 UV–Vis–NIR). The structural properties of ZnO/g-C_3N_4 NC were investigated using an IPD3000 X-ray diffractometer (XRD) with Cu anode source (line focus) operating at 40 kV and 30 mA, coupled to a multilayer collimating monochromator (Goebel mirror).

2.4. Photocatalytic degradation of ciprofloxacin

Lab experiments were performed with different ZnO/Melamine mass ratios synthesized coatings (1:10, and 1:20). The supported catalyst coating was inserted into a specific "in-house" developed reactor (Fig. S1, Supplementary Information) and fixed by a vacuum system. The support was a stainless-steel frame above which quartz window (Helios quartz NHI-1100) was placed with an inlet and an outlet to allow the water solution to flow laminarly on top of the catalyst. The distance between the quartz and the catalyst was 2 mm. The irradiation was provided by a solar simulator (LOT LS0306, with a Xenon lamp of 300W) with an installed filter to block radiation below 400 nm, and the illuminated surface is a circle with a diameter of 40 mm. The total circulated solution volume from a reservoir was 50 mL containing CIP (C_0 = 10 ppm) in a circuit flow of 1 L/h. The coatings were kept in the dark for the initial 30 min to achieve adsorption-desorption equilibrium and then irradiated for 180 min under photocatalytic conditions. 1 mL samples were taken at −30 min (dark) and illumination at 15, 30, 45, 60, 90, 120, 150, and 180 min, and absorption UV–vis spectra were recorded to evaluate the extent of CIP disappearance. The $\lambda_{max} = 276$ nm was used to probe the CIP removal/disappearance (Eq. (1)) by using a VARIAN Cary 5000 UV–Vis–NIR spectrophotometer over a wavelength range of 200–400 nm (Tozar et al., 2021).

$$\text{Degradation efficiency } (\%) = \left(\frac{C_o - C_t}{C_o}\right) \times 100 = \left(\frac{A_o - A_t}{A_o}\right) \times 100 \quad \text{Eq. 1}$$

Where C_0 and A_o are the starting molar concentration and absorbance of CIP while C_t and A_t are the molar concentration and absorbance of CIP at time t. The k - rate constant of the pseudo first-order reaction (appropriate for antibiotics degradation (Manasa et al., 2021)) is defined as:

$$-\ln\left(\frac{C_t}{C_o}\right) = kt$$

Using the optimum mass ratio photocatalyst determined in the lab, the material was then used for scale-up experiments with concentrated sunlight. The experiments were performed using a PTC designed and realized in-house (Fig. 2): the apparatus is based on a 1 m^2 parabolic mirror supported by a solar tracker and hosting a quartz tube photoreactor. A custom-made stainless steel sample holder (Fig. S2) capable of supporting up to 10 slides (75 × 25 mm) is positioned in the focus and liquid flow is sustained and regulated by a peristaltic pump (Seko, KRFF0210). The design and a complete technical description of the system can be found elsewhere (El Golli et al., 2024). Using a 5L volume of 10 ppm CIP solution, for appropriate scaling of the lab protocol, the liquid was circulated for 30 min to fill all the quartz tube and stabilize a continuous flow. After this time the solar concentrator was started to track the sunlight for 210 min. The experiments were performed between April and October 2023 in Trento-Italy, coordinates 46.06640° N, 11.15072° E between 10:00 and 14:00 local time. Solar irradiance measurements were conducted using a pyrheliometer (Kipp & Zonnen, model CHP1). To ensure consistency in experiments, they were carried out under conditions where irradiance levels fell within the range of 600–700 W/m^2. Reusability of photocatalyst: two degradation cycles of CIP were conducted to assess the reusability of the catalysts. Following each recycling experiment, the 10 photocatalyst slides were collected, dried, and subsequently reused under similar conditions for an additional test. Each time, randomly selected slides were checked for loss of coating material by weighing on a micro balance (10^{-5} g readability). The catalysts have been subjected to approximately 8 h total of circulation (sum dark and illuminated).

2.5. Assessment of antibacterial activity in CIP water samples

The residual antibacterial activity of the CIP water sampled before, during and after solar photocatalytic treatment was assessed on the CIP-sensitive bacterial laboratory strains *E. coli* K12 DSM 498, *P. megaterium*

Fig. 2. PTC apparatus used in this work.

MS941, *S. aureus* ATCC25923, *P. aeruginosa* PA14.

Briefly, each bacterial strain was tested individually and the assay was performed in transparent 96-well plates with flat-bottom (Sarstedt) by dispensing in each well 100 µL of water samples, previously filtered/sterilized with 0.2 µm filters (Sarstedt), and 100 µL of LB to allow bacterial growth. The 4 bacteria were previously grown overnight at 37 °C with 200 rpm shaking in LB and resuspended in LB at a density of approximately $2*10^7$ CFU/mL; 5 µL of these bacterial suspensions were added to each well, resulting in an inoculum size of approximately 10^5 CFU per well. Each bacterial strain was separately inoculated in a single plate to avoid contamination between bacteria. The plates were covered with Breathe-Easy® sealing membranes (Merck) and incubated for 24 h at 37 °C. Finally, bacterial growth was determined by optical density measurements at a wavelength of 600 nm (OD600) using a plate reader (Tecan Infinite 200 Microplate Reader).

Using the same method, bacterial sensitivity to CIP was also determined by measuring for each individual strain the antibiotic minimal inhibitory concentration (MIC) completely preventing bacterial growth. In this case, twofold serial dilutions of the antibiotic were made in sterile water (from 10 mg/L to 0.005 mg/L) and 100 µL of CIP solutions + 100 µL of LB were dispensed in each well before the addition of bacterial suspensions.

2.6. HPLC-MS of the photodegradation process

The degradation medium was analyzed by liquid chromatography (Model 1100 Series, HP) coupled to a photodiode-array detector (Model Agilent, 1100 Series, PDA), and to a mass spectrometer (Bruker Esquire-LC quadrupole ion trap) in positive-ion-mode Electrospray ionization source (ESI +). The chromatographic separation was carried out on a C18 column at 303 K (Phenomenex Kinetex C18 2.6um 100A (100 × 4.6 mm); flow 0.8 ml/min; T = 30 °C; injected volume = 10 µl). The mobile phase consisted of a 80/20 water/acetonitrile mixture with 0.1% of trifluoracetic acid. The DataAnalysis 3.0 software was used to integrate the collected ion chromatograms from the positive-ion full scan mode (50–500 Da) for the structural assignment of species (Bruker Daltonik, Bremen, Germany). A working curve of the available standard of CIP was built by recording UV (λ = 278 nm) peak areas for several solutions of CIP obtained by sequential dilution of a 10 mg/L mother solution.

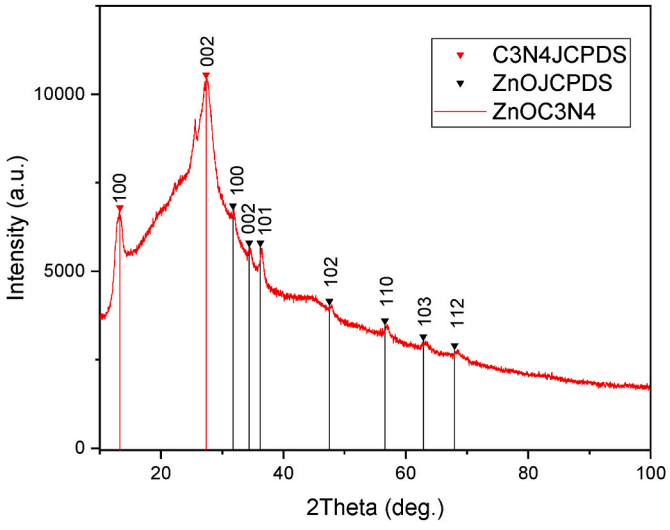

Fig. 3. XRD pattern of ZnO/g-C $_3$ N $_4$.

3. Results and discussion

3.1. Characterization of ZnO/g-C_3N_4 NC coatings

3.1.1. XRD analysis

Fig. 3 depicts the investigation of the crystalline structure of ZnO/g-C_3N_4 NC. The XRD peaks of the ZnO/g-C_3N_4 NC closely resembled those of graphitic carbon nitride and zinc oxide. The diffraction peaks at 2θ = 31.7, 34.4, 36.3, 47.5, 56.6, 62.8, 66.3, 67.9, 69.1, 72.7, and 76.9, displayed to the planes (100), (002), (101), (102), (110), (103), (200), (112), (201), (004) and (202), respectively, confirming the hexagonal crystal structure of ZnO as referenced from JCPDS card No. 36–1451 (El Golli et al., 2021). Some of the peaks appear shifted toward higher angles, likely indicating changes induced by composite formation (Van Thuan et al., 2022; Thangavelu et al., 2024; Liu et al., 2019; Tamilarasu et al., 2024). Two pronounced peaks at 13.3° and 27.5° are found, which are attributed to the graphitic phase carbon nitride as per standard JCPDS 87–1526 card. The lower-angle diffraction peak at 13.3° corresponds to tri-s-triazine units (100), while the stronger peak at 27.52° arises from the interlayer stacking of aromatic segments (002).

3.1.2. UV–visible spectrophotometry

The analysis of ZnO/g-C_3N_4 through UV–Vis diffuse reflectance spectra (DRS) gives insights into the composite's light absorption characteristic (Fig. 4a and b). The optical band gap of the composite was estimated through $F(R)h\nu$ (Kubelka-Munk function) plotted against $h\nu$ (photon energy), via the equation:

$$F(R)h\nu = A\left(h\nu - E_g\right)^n$$

where R is diffuse reflectance, $F(R) = \frac{(1-R)^2}{2R}$, A is an arbitrary coefficient, h is Planck's constant, ν is the light frequency, n = ½ (direct transition), and Eg is the optical bandgap (Luu Thi et al., 2021).

Pure ZnO has a reflectance edge at 377 nm, while the ZnO/g-C_3N_4 NC clearly extends its reflectance edge into the visible light range to about 433 nm. The extracted bandgaps of ZnO and ZnO/g-C_3N_4 NC are 3.19 eV and 2.86 eV respectively (Uma et al., 2017). This widened light absorption capacity in the ZnO-g-C_3N_4 composite allows for efficient utilization of visible light, implying its potential for sunlight-driven catalytic reaction. The decrease in band gap is generally attributed in literature to the modified optical band gap edges resulting from the interface interaction between g-C_3N_4 and ZnO electronic structures: exchange interactions involving s – d and p – d orbitals, causing a downward shift in the conduction band edge and an upward shift in the valence band edge (Uma et al., 2017; Girish et al., 2023; Jo and Clament Sagaya Selvam, 2015; Sun et al., 2012). Also, the synergistic effects of ZnO/g-C_3N_4 composite are reported to influence the lifetime of photogenerated charge carriers by effectively reducing internal charge recombination (Nie et al., 2018).

3.1.3. FT-IR analysis

FT-IR spectra are reported in Fig. 5. Transmittance peak in the range of 400–600 cm^{-1} related to stretching vibrations of Zn–O, and additional signals due to the presence of functional groups related to the garlic extract, were observed in the ZnO spectrum (Zhang et al., 2021). For pure g-C_3N_4, the peaks observed at approximately 1241, 1319, 1411, and 1461 cm^{-1} originate from the aromatic C–N stretching vibrations, whereas the C=N stretching vibrations could be found at 1569 and 1650 cm^{-1} (Ye et al., 2020; Narkbuakaew and Sujaridworakun, 2020; Jabar et al., 2022). The intense peak at 801 cm^{-1} exhibited the bending vibration of the s-triazine ring indicating the complete skeleton g-structure of g-C_3N_4. Two absorption bands (3415, and 3106 cm^{-1}) were regarded as the stretching and bending vibrations of N–H which come from the uncondensed terminal amino groups of g-C_3N_4 (Jabar et al., 2022; Wang et al., 2019, 2021a; Nikookar et al., 2021). The ZnO/g-C_3N_4 NC shows peaks from both ZnO and g-C_3N_4. The peaks in the FTIR spectrum of the

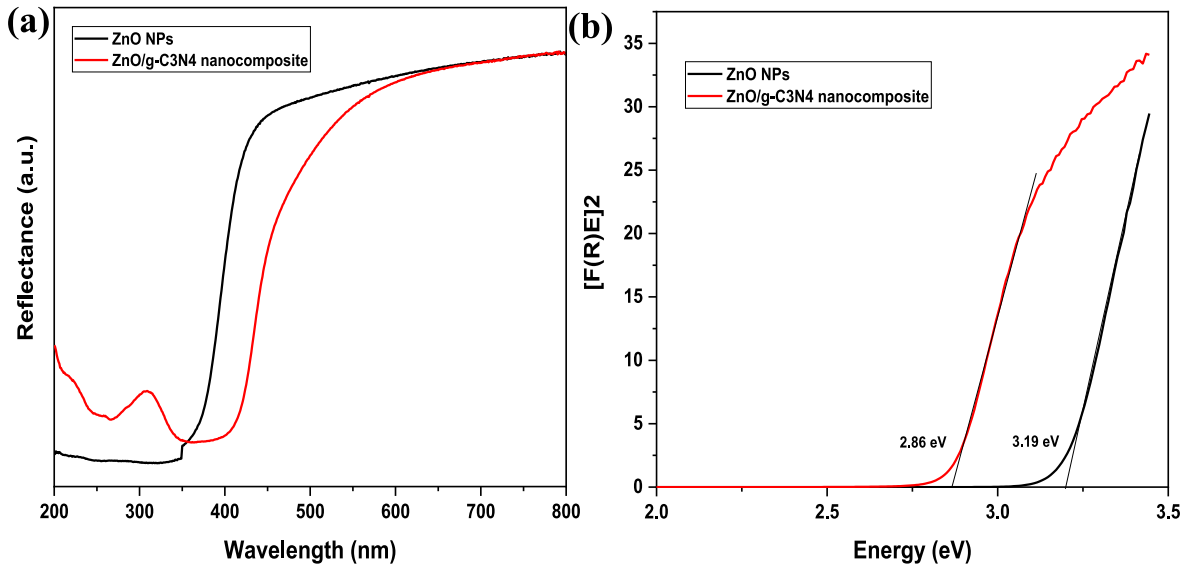

Fig. 4. (a) UV–Vis Reflectance spectra, and (b) corresponding Kubelka-Monk $[F(R)h\upsilon]^2$ plots of ZnO NPs, and ZnO/g-C_3N_4 NC.

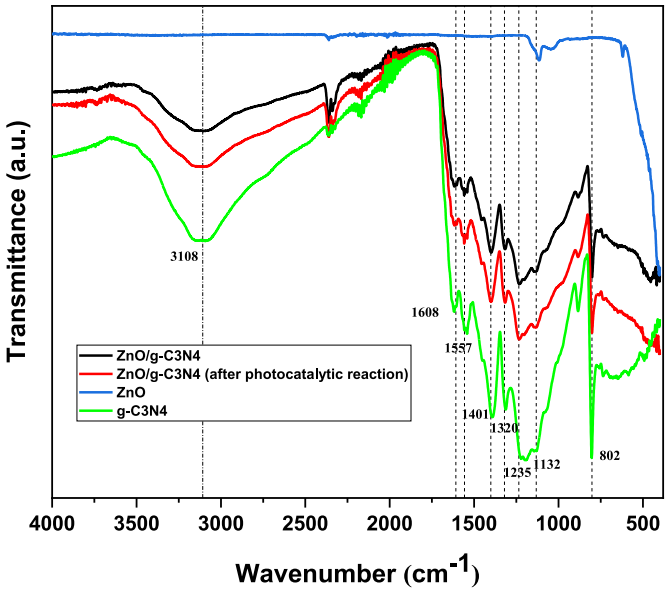

Fig. 5. FTIR spectra of ZnO, g-C_3N_4, and ZnO/g-C_3N_4 NC coating before and after degradation of CIP.

ZnO/g-C_3N_4 NC did not change after the photocatalytic degradation of CIP, thus proving the chemical stability of the composite (Suhag et al., 2023) (see Fig. 5).

3.1.4. FESEM- EDXS analysis

Fig. 6a depicts FESEM images illustrating the *in-situ* growth of g-C_3N_4 on green-synthesized ZnO NPs, exhibiting particle with sub-micron size (Sher et al., 2021). After 1 h of annealing at 550 °C, the ZnO/g-C_3N_4 nanocomposite exhibited a clearer foamy structure by coupling with the g-C_3N_4, probably because of the impact of gases discharged from melamine decomposition during the thermal condensation reaction (Sun et al., 2012) (Fig. 6b). The SEM image in Fig. S3 shows hetero nanoparticles with two different phases combining each other closely (Garg et al., 2021; Hakimi-Tehrani et al., 2021).

From the cross-sectional micrograph of ZnO/g-C_3N_4 NC (Fig. 7(a and b)), agglomeration of the Green ZnO particle in grains led to an opened structure of densely packed particles coated with a g-C_3N_4 layer, and the coating thickness is about 60 μm. EDXS spectroscopy was carried out to elucidate the surface elements composition of the as-prepared samples. Fig. S4 (a-b) of the Supplementary Information displays the distinctive and strong peaks of C, N, Si, Zn, and O atoms indicating the coexistence of these elements on the surface of the ZnO/g-C_3N_4 NC. Additional peaks for K, P, and S attributed to the garlic extract were recognized, in line with the composition of the Green ZnO powder used to produce the coatings (El Golli et al., 2021).

3.2. Solar photocatalysis - ZnO/g-C_3N_4 NC coatings

3.2.1. Laboratory scale

The effect of mass ratio in the ZnO/g-C_3N_4 coatings (1:10, 1:20) for the photocatalytic degradation is studied with an initial concentration of 10 ppm of CIP and illustrated in Fig. 8. The analysis was not performed on sample 1:60 because of its excessive roughness and apparent detachments due to the high amount of melamine precursor.

The ZnO/g-C_3N_4 coating with a 1:20 mass ratio presents increased adsorption in comparison to a 1:10 mass ratio. A greater adsorption rate can be linked to the increased production of surface hydroxyl radicals. These radicals form a water-absorbent layer on the catalyst, enhancing the interaction between the catalyst and the pollutant. The surface, which has adsorbed water, serves as a trap for photoexcited holes and aids in generating hydroxyl radicals by adsorbing OH– ions (Manasa et al., 2021). The enhanced photocatalytic activity of 1:20 mass ratio in ZnO/g-C_3N_4 coating under solar simulator, can be attributed, at least initially, to its improved adsorption capability resulting in more effective contact between the catalyst and the pollutant (see Fig. 8 at time 0, taken after 30 min of circulation under dark).

3.2.2. Solar concentrator

To evaluate the degradation of CIP at scaled-up experiments, results under solar concentrator apparatus are presented in Fig. 9. Based on HPLC data studies, the sunlight-mediated degradation efficiency was higher for the CIP solution in presence of 10 slides ZnO/g-C_3N_4 NC coatings (100% degradation efficiency and $k = 0.02113\ min^{-1}$) than the one exposed to only concentrated sunlight (55.5% degradation efficiency and $k = 0.00415\ min^{-1}$) during 210 min, resulting in earlier significant disappearance of the CIP (0.5 ppm) (Fig. 9(a)–(b)). The performance of the system, along with results from previous studies, is summarized in Table S1.

For practical implementation, the pivotal factors to be considered are reusability and mechanical stability. A preliminary recycling experiment

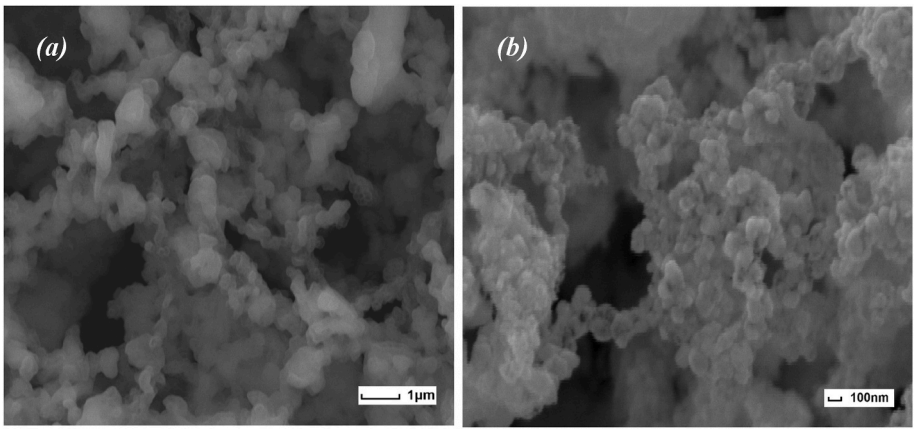

Fig. 6. FESEM images of ZnO/g-C_3N_4 NC coating (a) upon reaching 550 °C and (b) after 60 min of annealing at 550 °C.

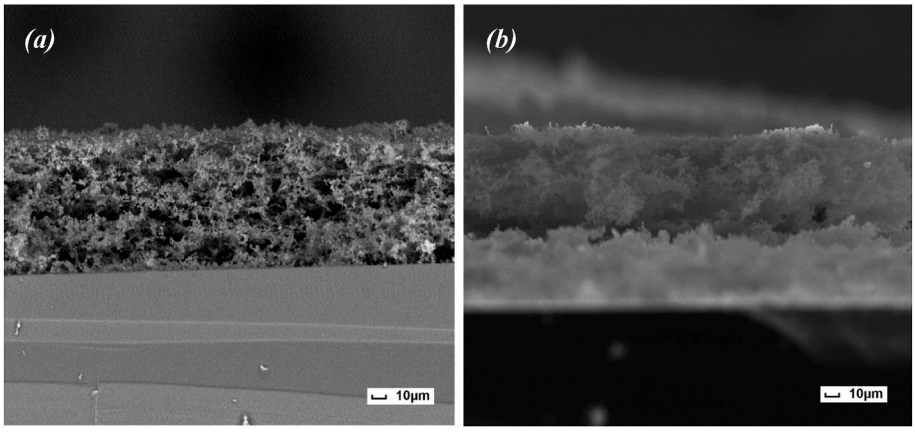

Fig. 7. Cross-section cut of ZnO/g-C_3N_4 NC coating (a) upon reaching 550 °C and (b) after 60 min of annealing at 550 °C.

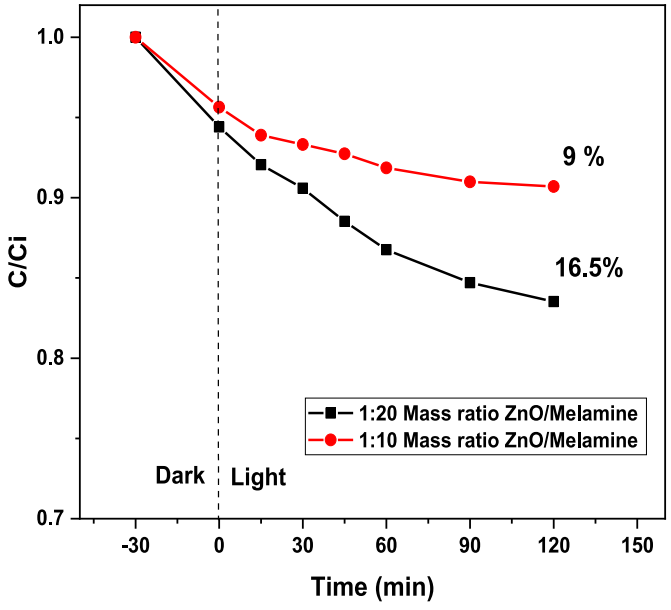

Fig. 8. Efficiency on 10 ppm CIP degradation of ZnO/g-C_3N_4 NC coating with two different mass ratios ZnO/Melamine (1:10, and 1:20) under solar simulator.

was performed under concentrated sunlight in the same conditions and a freshly prepared pollutant solution was used. The degradation pattern of the catalysts for CIP antibiotic for the second cycle was 89 % in 180 min (Fig. 10), which was about 10% less than the one obtained in the first cycle (99%).

To assess the stability of the films in terms of adhesion, coated-slides were weighed before and after each experiment using a micro balance (10^{-5} readability), showing no loss of material and thus demonstrating optimal mechanical stability. Given this result, the loss in photocatalytic efficiency, which can be considered good in the field, is likely due to fouling of the surface. A surface analysis technique such as FT-IR could reveal eventually adsorbed organic fragments, in which case regeneration could be obtained by simple calcination, washing with appropriate solvents or a combination of both. A more in-depth investigation of the surface after longer term use of the coatings is necessary and will be undertaken in the near future, to evaluate how to avoid the loss of efficiency and regenerate the material.

The reduction in the bandgap of ZnO/g-C_3N_4 NC allows the photon absorption also in the visible light region. In literature, it is proved that g-C_3N_4 acts as an electron acceptor facilitating charge separation in composites, as we used here. Visible light absorption and charge separation both contribute to enhanced photocatalytic performance (Suhag et al., 2023; Van Thuan et al., 2022; Wang et al., 2021b; Hassan et al., 2024). Indeed, upon excitation, the photogenerated electrons in the conduction band of g-C3N4 can migrate to the conduction band of ZnO, while the corresponding holes are left in the valence band of g-C3N4, thus permitting efficient charge separation. The electrons accumulated in the conduction band of ZnO may reduce adsorbed oxygen (O_2) to

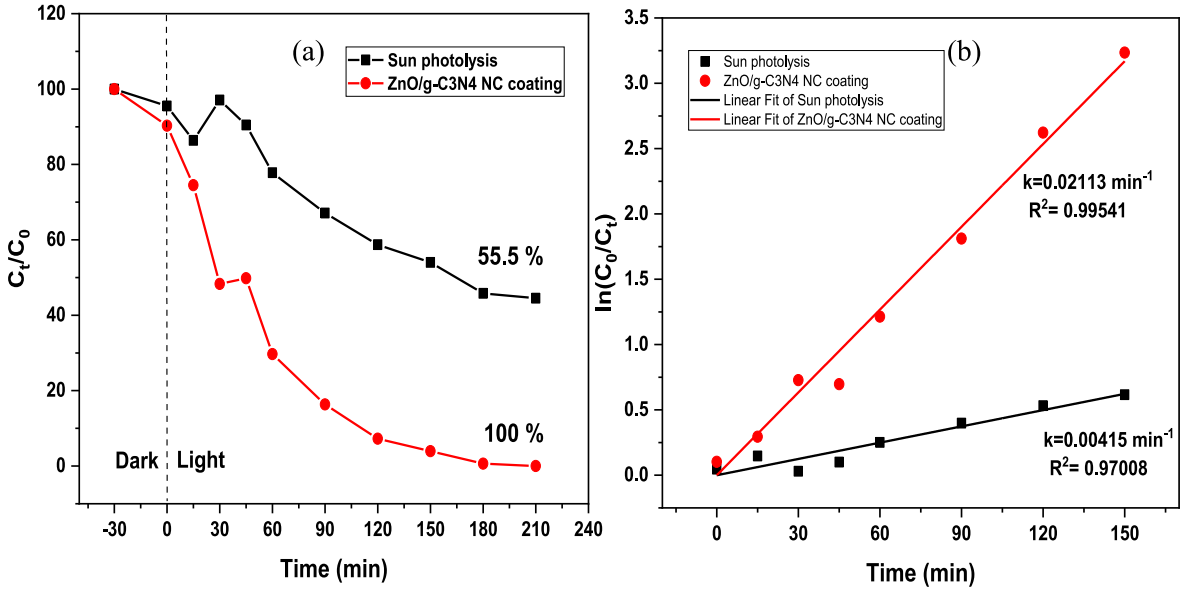

Fig. 9. Efficiency on 10 ppm CIP degradation of sun photolysis, 10 slides ZnO/g-C_3N_4 NC coating in scaled-up solar concentrator, determined by HPLC-MS.

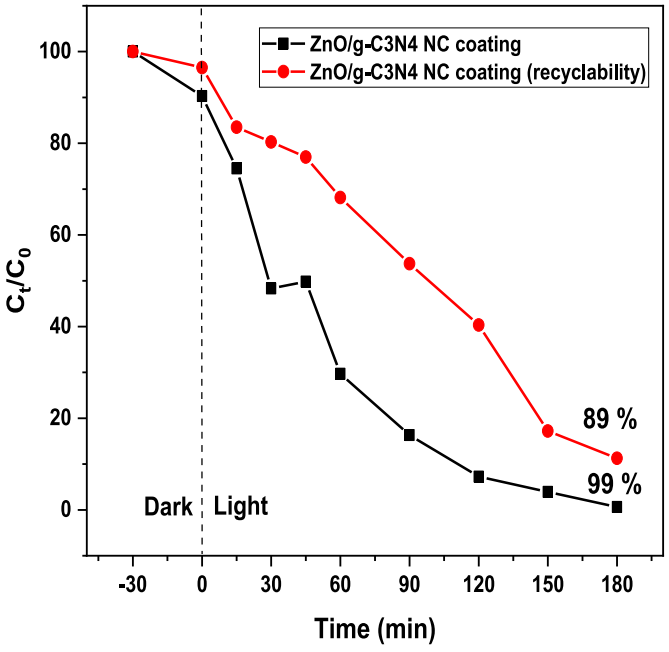

Fig. 10. Recyclability studies: Degradation (%) in a consecutive second photocatalytic cycle.

generate reactive oxygen species (superoxide radicals), which subsequently contribute to the oxidative degradation of antibiotics. The holes left in the valence band of g-C3N4 may directly oxidize antibiotic molecules (Suhag et al., 2023; Wang et al., 2021b).

3.2.3. *Identification of photocatalysis products by LC-MS*

Fig. 11 shows the most relevant chemical species observed by LC-MS (Fig. S5, Supplementary Information) during the oxidation of ciprofloxacin (CIP). Such architectures were tentatively assigned by studying their mass spectrum and by comparing them with previously reported literature (Bazzanella et al., 2023; Rehm and Rentsch, 2020). All the proposed structures are consistent with the typical degradation pathway resulting from the interaction of CIP with hydroxyl radical produced by the photocatalytic process in water.

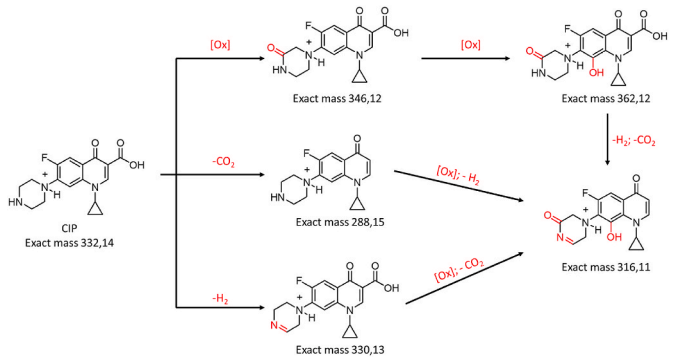

Fig. 11. Tentative degradation pathway of CIP during the photocatalytic process according to LC-MS analysis.

Three main processes were observed during photooxidation.

- Addition of oxidized moieties due to the presence of reactive radical oxygen species;
- Decarboxylation of the carboxylic acid with the consequent formation of CO_2;
- Hydrogen elimination as the result of radical oxidation.

Some observed species presenting masses of m/z values of 316, and 362, may also be the result of the combination of multiple oxidative processes. Although no clear indication of CIP mineralization can be indicated by LC-MS analysis, the photocatalytic process is clearly responsible for CIP major structural modifications that may be sufficient in inactivating the antibiotic behavior of the molecule.

3.3. *Residual antibiotic activity*

As previously mentioned, CIP is an antibiotic classified under the Fluoroquinolone (FQ) category. Antibiotics within this group typically hinder the growth of various microorganisms by targeting DNA Gyrase, a factor essential for bacterial cell division. Ciprofloxacin demonstrates activity against a broad spectrum of both Gram-positive and Gram-negative bacteria (Das et al., 2018). Therefore, the complete inactivation of the antibiotic within our experimental system was evaluated on the Gram-positive bacteria *P. megaterium* and *S. aureus*, and on the

Gram-negative bacteria *E. coli* and *P. aeruginosa*.

The MIC values of CIP were 0.02 mg/L for *E. coli* and 0.16 mg/L for *P. megaterium*, *S. aureus* and *P. aeruginosa* (the bacterial sensitivity to different concentration of CIP is plotted in Fig. S6). Therefore, all the bacteria were not resistant to CIP and *E. coli* resulted the most sensitive within the 4 strains.

After treating 10 ppm of CIP with ZnO/g-C_3N_4 NC coatings under sunlight, the residual antibacterial activity was assessed by measuring bacterial growth of each individual strain (Fig. 12 conditions c-d), and compared with untreated samples. The results of the experiments showed the loss of antibacterial activity in CIP water after 180 min of sunlight irradiation with ZnO/g-C_3N_4 NC coating photocatalyst. Indeed, the growth of *P. megaterium*, *S. aureus* and *P. aeruginosa* suggested that the CIP concentration present in treated water sample was <0.31 mg/L and the photocatalysis products did not have antimicrobial activity. However, under only concentrated sunlight exposure, no bacteria were able to grow in CIP water sampled before and after photolysis treatment (Fig. 12 conditions a-b). This clearly shows that CIP was still present in

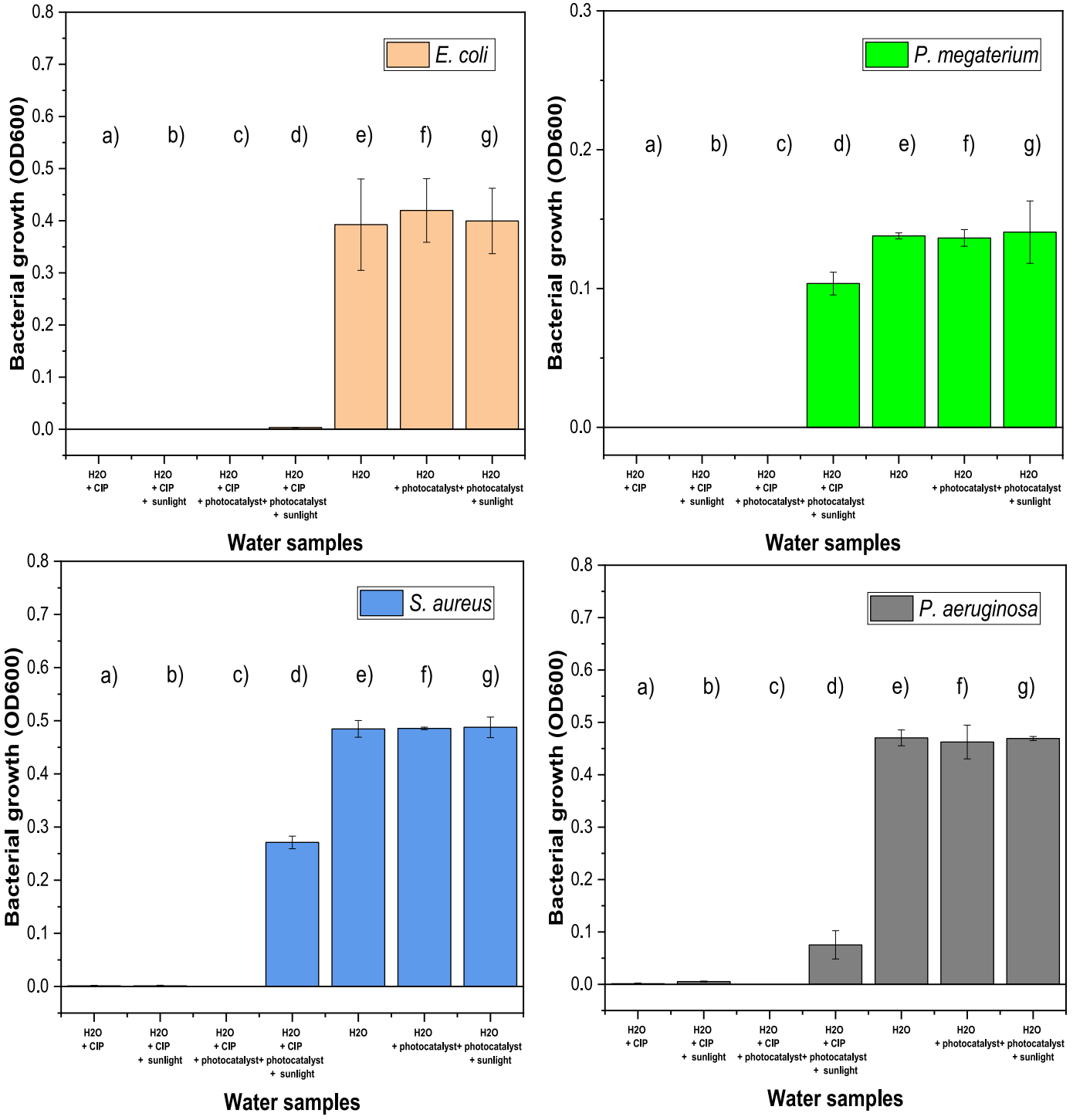

Fig. 12. Residual antibacterial activity of the 10 ppm CIP water collected pre- and post-180 min sunlight exposure alone (a–b) or with ZnO/g-C_3N_4 NC coating photocatalyst (c–d), assessed on growth of *E. coli*, *P. megaterium*, *S. aureus* and *P. aeruginosa*; bacterial growth tested in positive control samples without CIP, i.e., water, water + photocatalysts, and water + photocatalyst +180 min of sunlight irradiation (e–g).

the case of photolysis, indicating that both the photocatalyst (ZnO/g-C_3N_4) and concentrated sunlight are indispensable in the process. The positive control samples without CIP (water, water + photocatalysts, and water + photocatalyst + 180 min of sunlight irradiation) allowed the 4 bacteria growth, which ensured the elimination of any extra effects and confirmed the non-toxicity in water of the green synthesized photocatalyst (Fig. 12 conditions e-g).

These results were also confirmed by assessing bacterial growth in CIP water samples collected during the photocatalytic process (Fig. 13). In this case, 150 min of treatment were sufficient to allow both *S. aureus* and *P. aeruginosa* growth, while 180 min of treatment were necessary to reduce CIP concentration at a level allowing *P. megaterium* growth. In contrast, since *E. coli* is more sensitive to CIP compared with *S. aureus*, *P. aeruginosa* and *P. megaterium*, even 240 min of treatment were not sufficient to reduce CIP concentration at a level allowing *E. coli* growth. Finally, based on the sensitivity of each bacterium to CIP, we can hypothesize that the remaining CIP concentration after photo-catalysis treatment is between 0.04 and 0.31 mg/L. However, the initial CIP concentration used in this study (10 mg/L) is presumed to surpass the levels typically present in actual wastewater; therefore, we assume that this treatment could reduce CIP at concentration below 0.04 mg/L, allowing *E. coli* growth, when starting from a lower concentration of antibiotic (Das et al., 2018).

4. Conclusion

Concentrated solar light-driven photocatalytic inactivation of CIP using ZnO/g-C_3N_4 NC coatings has been carried out in this study. The photocatalysts synthesized by a simple *in-situ* thermal condensation method coupled with green synthesis (of ZnO) showed particle size in the nanoscale range. To evaluate the inactivation of ciprofloxacin, both spectrophotometric and microbiological (loss of antibiotic activity) methods were employed. During 210 min of photocatalytic process, 100% of the initial CIP (10 mg/L) was transformed under concentrated sunlight. The photocatalysts are found to be stable after a consecutive second recycle. The microbiological inactivation efficiency is found to

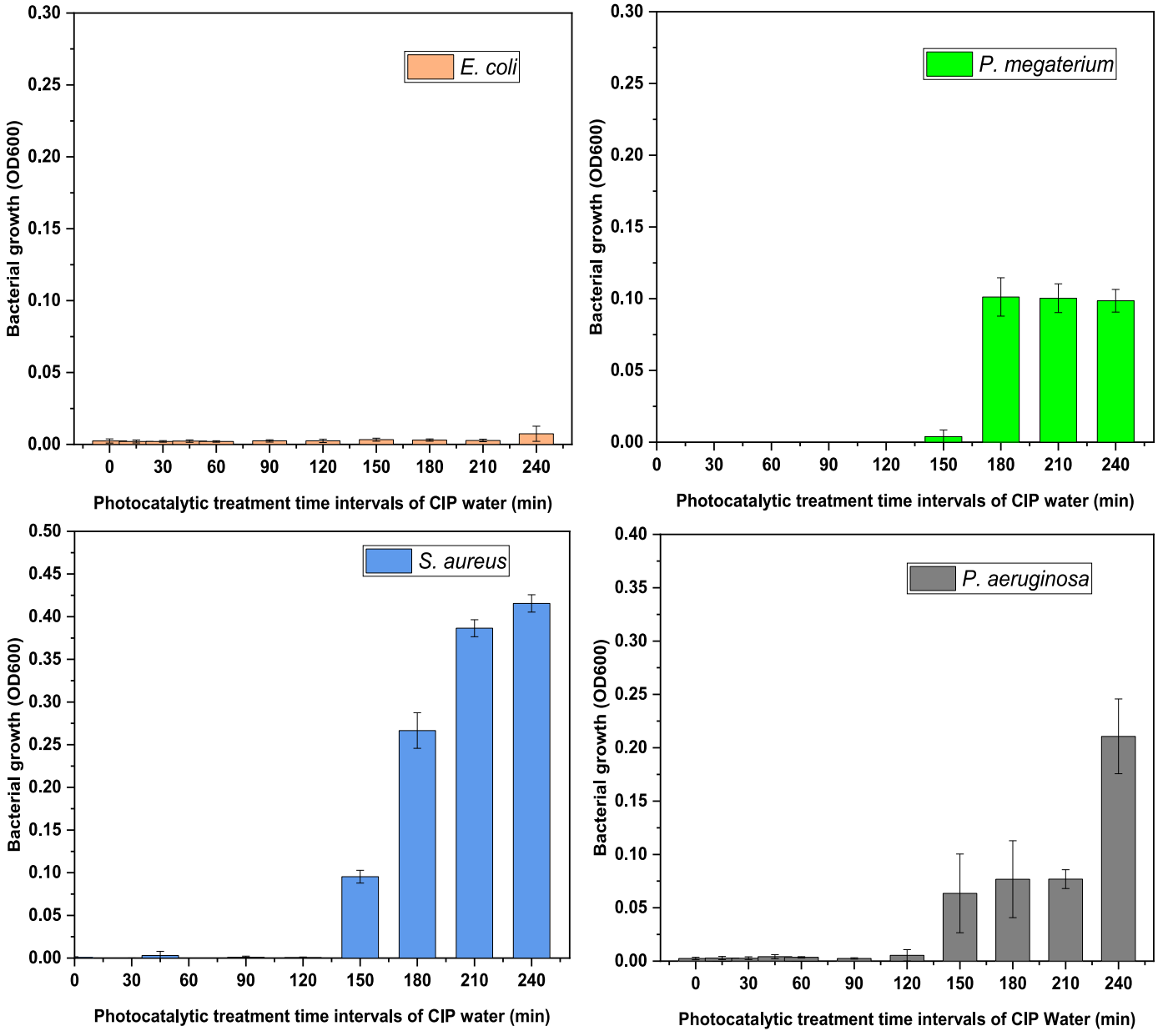

Fig. 13. Residual antibacterial activity of the 10 ppm CIP water collected during the time course of sunlight irradiation with ZnO/g-C3N4 NC coating photocatalyst, assessed on growth of *E. coli*, *P. megaterium*, *S. aureus* and *P. aeruginosa*.

be in the range of 96.9–99.6%. Thus, we successfully demonstrated the application of an immobilized, sunlight-activated green photocatalyst for sustainable treatment of emerging pharmaceuticals, aimed at AMR prevention. Also, the assessment of the remaining antibacterial activity after the treatment was conducted against multiple bacterial strains. It is significant to reflect that, although solar photocatalytic treatments are commonly aimed at complete pollutant removal by mineralization, the inactivation of antibiotic residues in water is sufficient for the likely reduction of AMR spread. In this work, a clear demonstration of this phenomenon is given through microbiological tests. We argue here that proving the antibiotic inactivation, a relatively underexplored aspect in current literature, is rather more important for our target application than focusing on mineralization and thus deserves further studies.

Although our study concentrates on a single antibiotic to offer in-depth insights, our results provide a solid foundation for evaluating photocatalytic wastewater treatment processes aimed at AMR prevention at scale. Building upon this, future research will address the complexities of real-world wastewaters, such as hospital effluents, where a mixture of antibiotics and other contaminants is likely present. To this end, the generally non-selective nature of photocatalysis-based processes may provide an advantage.

Our study also highlights the possible challenges arising from a perspective scale-up at industrial level. While using sunlight to power the process is definitely an advantage from an environmental perspective, solar irradiance is not only intermittent but also much variable with latitude and season. Thus, a solar wastewater treatment process should not be considered as a standalone technology but integrated in the flow of a WWTP. To this end, our demonstration of a 10 liter/h flow system is a step forward, even though the required flow rates in industrial settings are generally much higher. A possible solution would then be to consider our system as a single unit module, to be coupled with other modules to generate a solar field, possibly with single trackers supporting multiple PTCs and their photoreactors.

CRediT authorship contribution statement

Asma El Golli: Writing – original draft, Investigation, Conceptualization. **Davide Losa:** Writing – original draft, Investigation, Conceptualization. **Claudio Gioia:** Writing – original draft, Investigation. **Murilo Fendrich:** Writing – review & editing, Investigation. **Om Prakash Bajpai:** Methodology, Investigation. **Olivier Jousson:** Supervision, Conceptualization. **Michele Orlandi:** Writing – review & editing, Supervision, Methodology, Investigation, Funding acquisition, Conceptualization. **Antonio Miotello:** Writing – review & editing, Funding acquisition, Conceptualization.

Declaration of competing interest

The authors declare that they have no known competing financial interests or personal relationships that could have appeared to influence the work reported in this paper.

Acknowledgments

This work was supported by project FarSol, funded by the Caritro Foundation (Research & Development 2020 Grant) and “Produrre Idrogeno in Trentino—H2@TN” (PAT-Trento). We thank Francesco Cazzaniga for useful discussions and Marco Bettonte, Nicola Bazzanella, Sandro Gadotti and Claudio Cestari for technical help.

Appendix A. Supplementary data

Supplementary data to this article can be found online at https://doi.org/10.1016/j.jenvman.2024.123178.

Data availability

Data will be made available on request.

References

Akhil, D., Lakshmi, D., Senthil Kumar, P., Vo, D.-V.N., Kartik, A., 2021. Occurrence and removal of antibiotics from industrial wastewater. Environ. Chem. Lett. 19, 1477–1507. https://doi.org/10.1007/s10311-020-01152-0.

Al-Buriahi, A.K., Al-shaibani, M.M., Mohamed, R.M.S.R., Al-Gheethi, A.A., Sharma, A., Ismail, N., 2022. Ciprofloxacin removal from non-clinical environment: a critical review of current methods and future trend prospects. J. Water Process Eng. 47, 102725. https://doi.org/10.1016/j.jwpe.2022.102725.

Apreja, M., Sharma, A., Balda, S., Kataria, K., Capalash, N., Sharma, P., 2022. Antibiotic residues in environment: antimicrobial resistance development, ecological risks, and bioremediation. Environ. Sci. Pollut. Res. 29, 3355–3371. https://doi.org/10.1007/s11356-021-17374-w.

Bajpai, O.P., El Koura, Z., Pucher, I., Orlandi, M., Miotello, A., 2023. Graphitic carbon nitride (g-C 3 N 4) modified carbon electrodes for electrochemical energy storage systems. J. Electrochem. Soc. 170, 116507. https://doi.org/10.1149/1945-7111/ad0e46.

Bazzanella, N., Bajpai, O.P., Fendrich, M., Guella, G., Miotello, A., Orlandi, M., 2023. Ciprofloxacin degradation with a defective TiO2-x nanomaterial under sunlight. MRS Commun 13, 1252–1259. https://doi.org/10.1557/s43579-023-00440-4.

Bora, L.V., Mewada, R.K., 2017. Visible/solar light active photocatalysts for organic effluent treatment: fundamentals, mechanisms and parametric review. Renew. Sustain. Energy Rev. 76, 1393–1421. https://doi.org/10.1016/j.rser.2017.01.130.

Chidhambaram, N., Ravichandran, K., 2017. Fabrication of ZnO/g-C3N4 nanocomposites for enhanced visible light driven photocatalytic activity. Mater. Res. Express 4, 075037. https://doi.org/10.1088/2053-1591/aa7abd.

Das, S., Ghosh, S., Misra, A.J., Tamhankar, A.J., Mishra, A., Lundborg, C.S., Tripathy, S. K., 2018. Sunlight assisted photocatalytic degradation of ciprofloxacin in water using fe doped zno nanoparticles for potential public health applications. Int. J. Environ. Res. Public Health. 15, 2440. https://doi.org/10.3390/ijerph15112440.

El Golli, A., Fendrich, M., Bazzanella, N., Dridi, C., Miotello, A., Orlandi, M., 2021. Wastewater remediation with ZnO photocatalysts: green synthesis and solar concentration as an economically and environmentally viable route to application. J. Environ. Manage. 286, 112226. https://doi.org/10.1016/j.jenvman.2021.112226.

El Golli, A., Contreras, S., Dridi, C., 2023. Bio-synthesized ZnO nanoparticles and sunlight-driven photocatalysis for environmentally-friendly and sustainable route of synthetic petroleum refinery wastewater treatment. Sci. Rep. 13, 20809. https://doi.org/10.1038/s41598-023-47554-2.

El Golli, A., Fendrich, M., Bajpai, O.P., Bettonte, M., Edebali, S., Orlandi, M., Miotello, A., 2024. Parabolic trough concentrator design, characterization, and application: solar wastewater purification targeting textile industry dyes and pharmaceuticals—techno-economic study. Euro-Mediterranean J. Environ. Integr. https://doi.org/10.1007/s41207-024-00531-1.

Fendrich, M., Bajpai, O.P., Edla, R., Molinari, A., Ragonese, P., Maurizio, C., Orlandi, M., Miotello, A., 2023. Towards the development of a Z-scheme FeOx/g-C3N4 thin film and perspectives for ciprofloxacin visible light-driven photocatalytic degradation. Appl. Sci. 13, 10591. https://doi.org/10.3390/app131910591.

Garg, R., Gupta, R., Bansal, A., 2021. Synthesis of g-C3N4/ZnO nanocomposite for photocatalytic degradation of a refractory organic endocrine disrupter. In: Mater. Today Proc. Elsevier Ltd., pp. 855–859. https://doi.org/10.1016/j.matpr.2020.10.787

Girish, Y.R., Udayabhanu, Byrappa, N.M., Alnaggar, G., Hezam, A., Nagaraju, G., Pramoda, K., Byrappa, K., 2023. Rapid and facile synthesis of Z-scheme ZnO/g-C3N4 heterostructure as efficient visible light-driven photocatalysts for dye degradation and hydrogen evolution reaction. J. Hazard. Mater. Adv. 9, 100230. https://doi.org/10.1016/j.hazadv.2023.100230.

Guan, R., Li, J., Zhang, J., Zhao, Z., Wang, D., Zhai, H., Sun, D., 2019. Photocatalytic performance and mechanistic research of ZnO/g-C3N4 on degradation of methyl orange. ACS Omega 4, 20742–20747. https://doi.org/10.1021/acsomega.9b03129.

Hakimi-Tehrani, M.J., Hassanzadeh-Tabrizi, S.A., Koupaei, N., Saffar-Teluri, A., Rafiei, M., 2021. Facile thermal synthesis of g-C3N4/ZnO nanocomposite with antibacterial properties for photodegradation of Methylene blue. Mater. Res. Express 8, 125002. https://doi.org/10.1088/2053-1591/ac3c71.

Hartmann, A., Alder, A.C., Koller, T., Widmer, R.M., 1998. Identification of fluoroquinolone antibiotics as the main source of umuC genotoxicity in native hospital wastewater. Environ. Toxicol. Chem. 17, 377–382. https://doi.org/10.1002/etc.5620170305.

Hassan, F., Backer, S.N., Almanassra, I.W., Ali Atieh, M., Elbahri, M., Shanableh, A., 2024. Solar-matched S-scheme ZnO/g-C3N4 for visible light-driven paracetamol degradation. Sci. Rep. 14, 1–16. https://doi.org/10.1038/s41598-024-60306-0.

Husain Khan, A., Abdul Aziz, H., Palaniandy, P., Naushad, M., Cevik, E., Zahmatkesh, S., 2023. Pharmaceutical residues in the ecosystem: antibiotic resistance, health impacts, and removal techniques. Chemosphere 339, 139647. https://doi.org/10.1016/j.chemosphere.2023.139647.

Jabar, G., Saeed, M., Khoso, S., Zafar, A., Saggu, J.I., Waseem, A., 2022. Development of graphitic carbon nitride supported novel nanocomposites for green and efficient oxidative desulfurization of fuel oil. Nanomater. Nanotechnol. 12, 184798042211063. https://doi.org/10.1177/18479804221106321.

Jingyu, H., Ran, Y., Zhaohui, L., Yuanqiang, S., Lingbo, Q., Nti Kani, A., 2019. In-situ growth of ZnO globular on g-C3N4 to fabrication binary heterojunctions and their

photocatalytic degradation activity on tetracyclines. Solid State Sci. 92, 60–67. https://doi.org/10.1016/j.solidstatesciences.2019.02.009.
Jo, W.K., Clament Sagaya Selvam, N., 2015. Enhanced visible light-driven photocatalytic performance of ZnO-g-C3N4 coupled with graphene oxide as a novel ternary nanocomposite. J. Hazard Mater. 299, 462–470. https://doi.org/10.1016/j.jhazmat.2015.07.042.
Le-Minh, N., Khan, S.J., Drewes, J.E., Stuetz, R.M., 2010. Fate of antibiotics during municipal water recycling treatment processes. Water Res. 44, 4295–4323. https://doi.org/10.1016/j.watres.2010.06.020.
Liu, D.Y., Dong, J.H., Liu, F.M., Gao, X.F., Yu, Y., Zhang, S.B., Dong, L.M., Guo, Y.K., 2019. Synthesis and photocatalytic performance of g-C3N4 composites. J. Ovonic Res. 15, 239–246.
Lizundia, E., Luzi, F., Puglia, D., 2022. Organic waste valorisation towards circular and sustainable biocomposites. Green Chem. 24, 5429–5459. https://doi.org/10.1039/d2gc01668k.
Luu Thi, L.A., Neto, M.M., Van, T.P., Nguyen Ngoc, T., Nguyen Thi, T.M., Nguyen, X.S., Nguyen, C.T., 2021. In situ g-C3N4@Zno nanocomposite: one-pot hydrothermal synthesis and photocatalytic performance under visible light irradiation. Adv. Mater. Sci. Eng. 2021, 1–10. https://doi.org/10.1155/2021/6651633.
Manasa, M., Chandewar, P.R., Mahalingam, H., 2021. Photocatalytic degradation of ciprofloxacin & norfloxacin and disinfection studies under solar light using boron & cerium doped TiO2 catalysts synthesized by green EDTA-citrate method. Catal. Today 375, 522–536. https://doi.org/10.1016/j.cattod.2020.03.018.
Md Rosli, N.I., Lam, S.-M., Sin, J.-C., Satoshi, I., Mohamed, A.R., 2018. Photocatalytic performance of ZnO/g-C3N4 for removal of phenol under simulated sunlight irradiation. J. Environ. Eng. 144, 1–12. https://doi.org/10.1061/(asce)ee.1943-7870.0001300.
Meena, P.L.A.L., Poswal, K., Surela, A.K., Saini, J.K., 2022. Fabrication of g-C3N4/ZnO nanoheterostructures for effective degradation of methylene blue dye under visible light irradiation. Res. Sq.
Narkbuakaew, T., Sujaridworakun, P., 2020. Synthesis of tri-S-triazine based g-C3N4 photocatalyst for cationic rhodamine B degradation under visible light. Top. Catal. 63, 1086–1096. https://doi.org/10.1007/s11244-020-01375-z.
Ngullie, R.C., Alaswad, S.O., Bhuvaneswari, K., Shanmugam, P., Pazhanivel, T., Arunachalam, P., 2020. Synthesis and characterization of efficient ZnO/g-C3N4 nanocomposites photocatalyst for photocatalytic degradation of methylene blue. Coatings 10, 500. https://doi.org/10.3390/coatings10050500.
Nie, N., Zhang, L., Fu, J., Cheng, B., Yu, J., 2018. Self-assembled hierarchical direct Z-scheme g-C3N4/ZnO microspheres with enhanced photocatalytic CO2 reduction performance. Appl. Surf. Sci. 441, 12–22. https://doi.org/10.1016/j.apsusc.2018.01.193.
Nikookar, M., Rezaeifard, A., Jafarpour, Maasoumeh, Grzhegorzhevskii, K.V., Ostroushko, A.A., 2021. A top-down design for easy gram scale synthesis of melem nano rectangular prisms with improved surface area. RSC Adv. 11, 38862–38867. https://doi.org/10.1039/d1ra07440g.
Rehm, S., Rentsch, K.M., 2020. LC-MS/MS method for nine different antibiotics. Clin. Chim. Acta 511, 360–367. https://doi.org/10.1016/j.cca.2020.11.001.
Salma, A., Thoröe-Boveleth, S., Schmidt, T.C., Tuerk, J., 2016. Dependence of transformation product formation on pH during photolytic and photocatalytic degradation of ciprofloxacin. J. Hazard Mater. 313, 49–59. https://doi.org/10.1016/j.jhazmat.2016.03.010.
Shariati, A., Arshadi, M., Khosrojerdi, M.A., Abedinzadeh, M., Ganjalishahi, M., Maleki, A., Heidary, M., Khoshnood, S., 2022. The resistance mechanisms of bacteria against ciprofloxacin and new approaches for enhancing the efficacy of this antibiotic. Front. Public Heal. 10. https://doi.org/10.3389/fpubh.2022.1025633.
Sher, M., Shahid, S., Javed, M., 2021. Synthesis of a novel ternary (g-C3N4 nanosheets loaded with Mo doped ZnOnanoparticles) nanocomposite for superior photocatalytic and antibacterial applications. J. Photochem. Photobiol. B Biol. 219, 112202. https://doi.org/10.1016/j.jphotobiol.2021.112202.
Suhag, M.H., Khatun, A., Tateishi, I., Furukawa, M., Katsumata, H., Kaneco, S., 2023. One-step fabrication of the ZnO/g-C3N4 composite for visible light-responsive photocatalytic degradation of bisphenol E in aqueous solution. ACS Omega 8, 11824–11836. https://doi.org/10.1021/acsomega.2c06678.
Sun, J.X., Yuan, Y.P., Qiu, L.G., Jiang, X., Xie, A.J., Shen, Y.H., Zhu, J.F., 2012. Fabrication of composite photocatalyst g-C 3N 4-ZnO and enhancement of photocatalytic activity under visible light. Dalt. Trans. 41, 6756–6763. https://doi.org/10.1039/c2dt12474b.
Tamilarasu, K., Ranjith, R., Priyadharsan, A., Rojviroon, T., Maadeswaran, P., Suganya, S., Umarani, C., 2024. Hierarchical MoS2–SnS2@g–C3N4 nanocomposite as an efficient and sustainable material for environmental remediation. J. Clust. Sci. 35, 561–573. https://doi.org/10.1007/s10876-023-02498-5.
Thangavelu, K., Rajendran, R., Palanisamy, S., Arumugam, P., Thammasak, R., 2023. Powerful combination of FeWO4/g-C3N4 heterostructures for solar light driven photocatalytic degradation of tetracycline and its antibacterial activity. Mater. Today Sustain. 24, 100562. https://doi.org/10.1016/j.mtsust.2023.100562.
Thangavelu, K., Abimannan, G., Rajendran, R., Arumugam, P., 2024. Crafting high-performance CuZnO2/g-C3N4 nanocomposites: unleashing the power of dual-functional photocatalysis and antibacterial action. Ionics 30, 4885–4899. https://doi.org/10.1007/s11581-024-05603-4.
Tozar, T., Boni, M., Staicu, A., Pascu, M.L., 2021. Optical characterization of ciprofloxacin photolytic degradation by UV-pulsed laser radiation. Molecules 26. https://doi.org/10.3390/molecules26082324.
Uma, R., Ravichandran, K., Sriram, S., Sakthivel, B., 2017. Cost-effective fabrication of ZnO/g-C3N4 composite thin films for enhanced photocatalytic activity against three different dyes (MB, MG and RhB). Mater. Chem. Phys. 201, 147–155. https://doi.org/10.1016/j.matchemphys.2017.08.015.
Van Doorslaer, X., Dewulf, J., Van Langenhove, H., Demeestere, K., 2014. Fluoroquinolone antibiotics: an emerging class of environmental micropollutants. Sci. Total Environ. 500–501, 250–269. https://doi.org/10.1016/j.scitotenv.2014.08.075.
Van Thuan, D., Nguyen, T.B.H., Pham, T.H., Kim, J., Hien Chu, T.T., Nguyen, M.V., Nguyen, K.D., Al-onazi, W.A., Elshikh, M.S., 2022. Photodegradation of ciprofloxacin antibiotic in water by using ZnO-doped g-C3N4 photocatalyst. Chemosphere 308, 136408. https://doi.org/10.1016/j.chemosphere.2022.136408.
Verlicchi, P., Al Aukidy, M., Galletti, A., Petrovic, M., Barceló, D., 2012. Hospital effluent: investigation of the concentrations and distribution of pharmaceuticals and environmental risk assessment. Sci. Total Environ. 430, 109–118. https://doi.org/10.1016/j.scitotenv.2012.04.055.
Wang, Z.T., Xu, J.L., Zhou, H., Zhang, X., 2019. Facile synthesis of Zn(II)-doped g-C 3 N 4 and their enhanced photocatalytic activity under visible light irradiation. Rare Met. 38, 459–467. https://doi.org/10.1007/s12598-019-01222-5.
Wang, L., Li, Y., Han, P., 2021a. Electrospinning preparation of g-C3N4/Nb2O5 nanofibers heterojunction for enhanced photocatalytic degradation of organic pollutants in water. Sci. Rep. 11, 22950. https://doi.org/10.1038/s41598-021-02161-x.
Wang, F., Zhu, Z., Guo, J., 2021b. 2D-2D ZnO/N doped g-C3N4composite photocatalyst for antibiotics degradation under visible light. RSC Adv. 11, 35663–35672. https://doi.org/10.1039/d1ra06607b.
Watkinson, A.J., Murby, E.J., Costanzo, S.D., 2007. Removal of antibiotics in conventional and advanced wastewater treatment: implications for environmental discharge and wastewater recycling. Water Res. 41, 4164–4176. https://doi.org/10.1016/j.watres.2007.04.005.
Wise, R., 2002. Antimicrobial resistance: priorities for action. J. Antimicrob. Chemother. 49, 585–586. https://doi.org/10.1093/jac/49.4.585.
Ye, C., Wang, R., Wang, H., Jiang, F., 2020. The high photocatalytic efficiency and stability of LaNiO3/g-C3N4 heterojunction nanocomposites for photocatalytic water splitting to hydrogen. BMC Chem 14, 65. https://doi.org/10.1186/s13065-020-00719-w.
Yu, J., Bao, P., Liu, J., Jin, Y., Li, J., Lv, Y., 2023. Cu and Ni dual-doped ZnO nanostructures templated by cellulose nanofibrils for the boosted visible-light photocatalytic degradation of wastewater pollutants. Green Chem. 25, 10530–10537. https://doi.org/10.1039/d3gc04163h.
Zhang, Y., Zhao, S.M., Su, Q.W., Xu, J.L., 2021. Visible light response ZnO–C3N4 thin film photocatalyst. Rare Met. 40, 1–9. https://doi.org/10.1007/s12598-019-01297-0.